Catalysis Today 164 (2011) 176–180

Contents lists available at ScienceDirect

Catalysis Today

journal homepage: www.elsevier.com/locate/cattod

The oxygen reduction electrocatalytic activity of intermetallic compound of palladium–tin supported on tin oxide–carbon composite

Seon-ah Jin[a], Kyungjung Kwon[a,b], Chanho Pak[a,*], Hyuk Chang[a]

[a] Energy Lab., Emerging Tech. Research Center, Samsung Advanced Institute of Technology, Samsung Electronics. Co., Ltd., San#14-1, Nongseo-dong, Giheung-gu, Yongin-si, Gyeonggi-do 446-712, Republic of Korea
[b] Department of Energy & Mineral Resources Engineering, Sejong University, Seoul 143-747, Republic of Korea

ARTICLE INFO

Article history:
Received 16 July 2010
Received in revised form 9 November 2010
Accepted 9 November 2010
Available online 8 December 2010

Keywords:
Fuel cell catalyst
Palladium
Tin oxide
Oxygen reduction
Intermetallic compound

ABSTRACT

Pd nanoparticles on tin oxide–carbon composite support (Pd/SnO_2–KB) are synthesized by sequential impregnation and successive reduction method. The Pd/SnO_2–KB catalyst is reduced at various temperatures and the evolution of phases such as intermetallic Pd_3Sn compound depending on temperature is characterized with XRD, TEM and XPS analyses. Pd/SnO_2–KB reduced at 700 °C and above temperatures exhibits the Pd–Sn intermetallic compound with a smaller particle size than Pd pure metal phase. Pd/SnO_2–KB reduced at 700 °C shows the highest oxygen reduction catalytic activity, which is attributed to the combined effect of the smaller oxygen binding energy of Pd and the increased oxygen adsorption affinity of Sn on the intermetallic Pd–Sn surface. The approach of improving electrocatalytic activity by forming an intermetallic compound can be attempted with various combinations of noble and transition metals.

1. Introduction

Proton exchange membrane fuel cell (PEMFC) is a promising candidate for power generation source for zero-emission vehicle and distributed power generation system. However, PEMFC has some critical obstacles such as cost and durability that must be solved for commercialization. Platinum catalyst, which has been known as the most active catalytic material so far, is one of the most expensive components in a fuel cell system. To replace Pt in the fuel cell system, relatively inexpensive palladium-based catalysts have been studied as cathode catalyst due to a comparable oxygen reduction electrochemical property to Pt [1]. To enhance the oxygen reduction reaction (ORR) activity of palladium-based catalysts, many approaches have been attempted including alloy formation [2–5], structure control [6], facet control [7] and the addition of transition and rare earth metal oxide co-catalysts [8–11].

The use of intermetallic compounds as ORR electrocatalyst can be considered because intermetallic compounds have generally an advantage over disordered alloys in terms of the controllability of the structural, geometric and electronic effects [12,13]. Casado-Rivera et al. identified the ordered intermetallic phases of PtBi, PtIn, and PtPb, which exhibited an enhanced electrocatalytic activity compared to Pt [12]. However, Pd-based intermetallic compounds have not been reported as ORR electrocatalyst to the best of our knowledge presumably because the conventional synthesis of intermetallic compounds prevents the formation of Pd-based intermetallic nanoparticles. In this study, Pd-based intermetallic nanoparticles are prepared by sequential impregnation and successive heat treatment where tin oxide is used as sintering barrier and secondary metal source. Further, the relation between the ORR activity and the surface composition of the Pd-based intermetallic nanoparticles are investigated.

2. Experimental

2.1. Catalyst synthesis

Pd catalyst supported on tin oxide–carbon composite (Pd/SnO_2–KB) was prepared by sequential impregnation method. First, the SnO_2-Ketjen black (Akzo Company, KB 300J) composite support was synthesized via conventional impregnation method from an aqueous solution of tin chloride ($SnCl_2 \cdot 2H_2O$, 62.6 wt.% Sn), which was purchased from Sigma–Aldrich. KB was dispersed in the tin chloride solution and the mixture was heated at 60 °C under vacuum to remove the solvent. Tin chloride-impregnated KB was dried at 80 °C for 12 h and calcined at 200 °C resulting in the formation of tin oxide–carbon composite (SnO_2–KB) support. Thirty wt.% of Pd was loaded on KB and SnO_2–KB, respectively

* Corresponding author. Tel.: +82 31 280 6884; fax: +82 31 280 9359.
E-mail address: chanho.pak@samsung.com (C. Pak).

0920-5861/$ – see front matter © 2010 Elsevier B.V. All rights reserved.
doi:10.1016/j.cattod.2010.11.027

by using palladium(II) nitrate ($Pd(NO_3)_2$•xH_2O, 40.2 wt.% Pd, Umicore) as precursor with the nominal Pd:Sn atomic ratio of 3:1. Palladium nitrate-impregnated supports were thermally reduced at various temperatures (300 °C, 500 °C, 700 °C and 900 °C) in a tube furnace under flowing hydrogen to form intermetallic compounds.

2.2. Catalyst characterization

Structural and morphological characterization was performed by X-ray diffraction (XRD) and transmission electron microscopy (TEM). Powder XRD patterns were collected by using a Philips X'pert Pro X-ray diffractometer and Cu-Kα radiation source. A G2 FE-TEM Tecnai microscope was used for the confirmation of particle size and distribution, which can be complementary to the information of mean particle size from XRD pattern. X-ray photoelectron spectroscopy (XPS) measurement was performed with an AXIS (Q2000) photoelectron spectrometer equipped with a monochromated Al-Kα source.

Electrochemical analysis was conducted by using rotating disk electrode (RDE) apparatus (Princeton Applied Research). Catalyst ink for working electrode was prepared by ultrasonically dispersing 20 mg of catalyst in 10 ml of deionized water. 15 μl of the catalyst ink was dropped onto a polished glassy carbon disk (surface area: 0.196 cm^2) and then 0.05 wt.% of Nafion solution (Aldrich) was adopted to fix the catalyst layer. A Pt-foil counter electrode and an Ag/AgCl reference electrode were used for electrochemical tests. Cyclic voltammetry (CV) was performed in the potential range between 0.05 V and 1.2 V *vs.* reversible hydrogen electrode (RHE) at a scan rate of 50 mV/s in N_2-saturated 0.1 M $HClO_4$ electrolyte. ORR activity was evaluated at a scan rate of 5 mV/s in O_2-saturated 0.1 M $HClO_4$ electrolyte at room temperature.

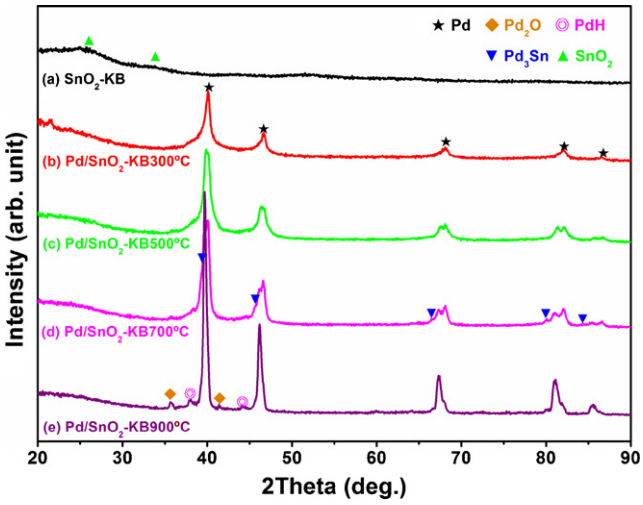

Fig. 1. XRD patterns of as-prepared (a) SnO_2–KB, (b) Pd/SnO_2–KB 300 °C, (c) Pd/SnO_2–KB 500 °C, (d) Pd/SnO_2–KB 700 °C and (e) Pd/SnO_2–KB 900 °C.

3. Results and discussion

3.1. Physical characterization of catalyst

The calcination condition for the synthesis of SnO_2–KB support was optimized to form nanoparticles of tin oxide on the carbon. After the calcination, SnO_2–KB shows very broad SnO_2 (JCPDS No. 41-1445) and carbon peaks from the XRD measurement (Fig. 1). The crystallite size of SnO_2 is about 3 nm, which was calculated from Sherrer equation using the uncoupled diffraction peak (1 0 1) of SnO_2. The estimated size was well matched with TEM analysis result. As shown in Fig. 2(a), the TEM image

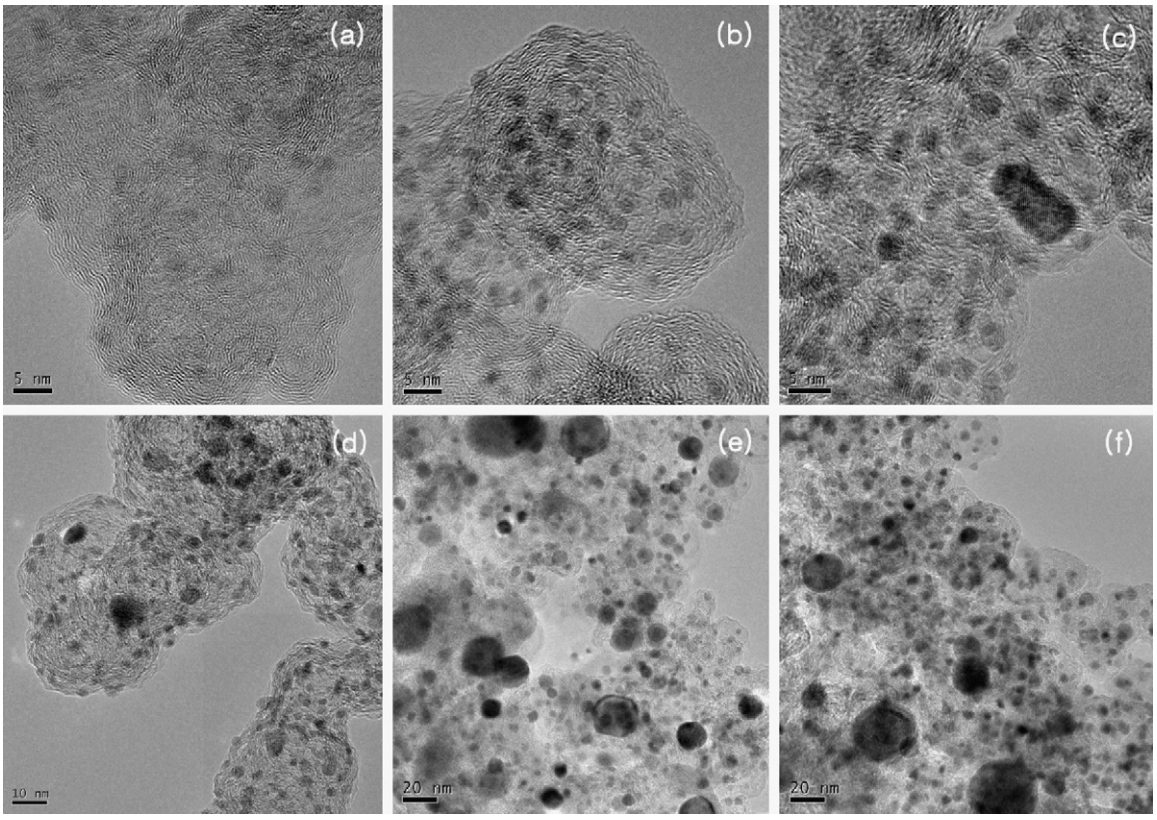

Fig. 2. TEM images of as-prepared (a) SnO_2–KB, (b) Pd/KB 300 °C, (c) Pd/SnO_2–KB 300 °C, (d) Pd/SnO_2–KB 500 °C, (e) Pd/SnO_2–KB 700 °C and (f) Pd/SnO_2–KB 900 °C.

Table 1
Characterization of Pd/KB and Pd/SnO_2–KB from XRD mesurement data.

	Pd/KB				Pd/SnO_2–KB				Phase
	300 °C	500 °C	700 °C	900 °C	300 °C	500 °C	700 °C	900 °C	
Pd-related peak position (2θ)	40.11	40.16	40.25	40.39	40.09	–	39.25	39.3	Ordered Pd_3Sn
						39.86	39.7	39.69	Sn-doped Pd
						40.11	40.04		Pd
Crystallite size (nm)	2.7	8.6	17.7	23.2	10.2		5.6	12.8	Ordered Pd_3Sn
						3.3	13.1	20.4	Sn-doped Pd
						10.0	17.6		Pd

indicates the SnO_2 particle size of about 1–4 nm. The SnO_2–KB support has a reduced surface area (440 m^2/g-support) compared to KB (804 m^2/g-support), of which surface area was estimated using BET method. The smaller surface area of SnO_2–KB support is partly because tin oxide blocks the micropores of KB and partly because SnO_2–KB is a composite of high surface area KB and low surface area metal oxide.

The XRD patterns of SnO_2–KB and Pd/SnO_2–KB catalysts reduced at various temperature (300 °C, 500 °C, 700 °C and 900 °C) are presented in Fig. 1. All Pd-loaded samples are identified as a face-centered cubic structure (JCPDS No. 46-1043). The Pd peaks are shifted toward lower degrees and start to split as the reduction temperature increases (Table 1), which indicates the expansion of Pd lattice caused by the interaction with Sn-containing species in the composite support. The peak separation of Pd diffraction pattern appearing at 500 °C indicates the separate formation of Pd and Sn-doped Pd phases and the peaks for intermetallic Pd_3Sn phase (JCPDS No. 03-065-8225) are clearly observed at higher temperatures (700 °C and 900 °C). The Pd_2O (JCPDS No. 03-065-5065) and PdH (JCPDS No. 03-065-0557) diffraction peaks are additionally observed at both Pd/KB (data not shown) and Pd/SnO_2–KB treated above 700 °C. PdH and Pd_2O might be decomposition products from impurities in ambient hydrogen at high temperatures.

The XRD patterns were deconvoluted and characterized in Table 1 to compare with the TEM images. The estimated Pd crystallite sizes of Pd/KB 300 °C and Pd/SnO_2–KB 300 °C are 2.7 nm and 10.2 nm (Table 1), respectively. Pd/KB 300 °C has a particle size distribution between 1.5 nm and 4 nm with the majority of particles having a size of ca. 2 nm from the TEM analysis. Pd/SnO_2–KB 300 °C and Pd/SnO_2–KB 500 °C show a very similar particle size distribution where most particles have 2–5 nm size and large particles of about 10 nm are infrequently observed as in Fig. 2(c) and (d). Because the estimated Pd crystallite size by the XRD analysis represents the mean particle size, the crystallite size in Table 1 might be larger than the most representative particle size in the TEM analysis particularly for Pd/SnO_2–KB, of which particle size distribution is wider than that of Pd/KB. There appears some convoluted XRD peaks assigned to Sn-doped Pd and ordered Pd_3Sn at higher temperatures as seen in Table 1. The peaks other than Pd pure metal phase lead to bimodal or trimodal particle size distributions at higher temperatures. While the trend in the particle size of Pd pure metal with increasing temperature is similar for both Pd/KB and Pd/SnO_2–KB, the corresponding particle sizes of Sn-doped Pd and ordered Pd_3Sn at the same temperature are smaller than that of Pd pure metal phase. In the TEM images of Fig. 2(e) and (f), Pd/SnO_2–KB 700 °C and Pd/SnO_2–KB 900 °C show bimodal or trimodal particle size distributions where agglomerated particles as large as 20 nm and relatively smaller groups of particles coexist.

The smaller particle sizes of Sn-doped Pd and ordered Pd_3Sn than that of Pd pure metal can be attributed to tin oxide acting as sintering barrier and secondary intermetallic source. The sintering of Pd particles at Pd/KB is accelerated as reduction temperature increases, whereas the particle sintering acceleration at Pd/SnO_2–KB is slowed down because of the evolution of intermetallic Pd_3Sn in between 500 °C and 700 °C. Takeguchi et al. investigated the reduction behavior of SnO_2 in contact with Pd metal (Pd/C/SnO_2) with temperature-programmed reduction method [14]. Tin in Pd/SnO_2–KB seems to actively participate in the formation of the Pd–Sn intermetallic compound after tin oxide is completely reduced at 580 °C based on their results on Pd/C/SnO_2, which has similar structural and compositional features to Pd/SnO_2–KB.

3.2. ORR activity and chemical characterization of catalyst

The ORR activities of Pd/KB and Pd/SnO_2–KB reduced at various temperatures are compared in Fig. 3. The ORR activity is often evaluated with the specific activity measured at a potential (herein 0.8 V) close to the onset potential of ORR. The information on the ORR kinetics is also reflected in the onset potential itself because a higher onset potential means a smaller overpotential for the ORR. First, a similar level of ORR activity is observed for Pd/KB 300 °C and Pd/SnO_2–KB 300 °C. This result supported that the Pd particles of pure metal state are exclusively formed regardless of SnO_2 addition to KB at this temperature as in Table 1. Second, the catalyst treated at 700 °C among Pd/SnO_2–KB series shows the highest activity in terms of both specific activity and onset potential. It might be worth mentioning that its ORR onset potential of 0.88 V is still below that of a commercial Pt/C (for example, 0.95 V of Pt(28.3%)/C from Tanaka Kikinzoku Kogyo).

The tendency of ORR activity of the catalysts will be correlated with the following XPS analysis. The Pd/KB catalyst exhibits the binding energy centered at 335.8 eV for Pd $3d_{5/2}$ in Fig. 4(a), which can be matched with the reported Pd 3d binding energy of 2.7 nm Pd nanoparticles [15]. For the Pd/SnO_2–KB catalysts except the 900 °C-

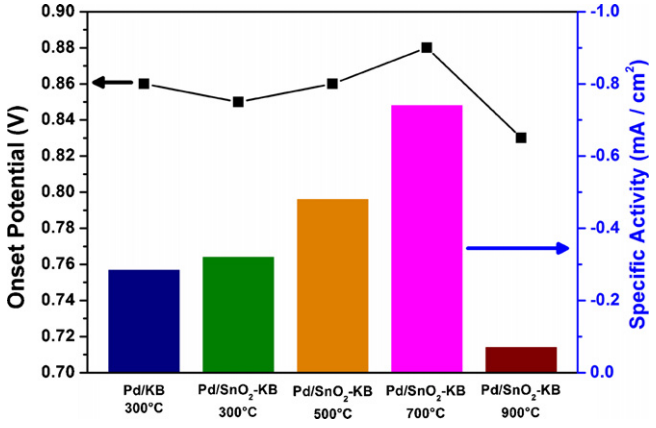

Fig. 3. Comparison of oxygen reduction onset potential and specific activity at 0.8 V of Pd/KB 300 °C and Pd/SnO_2–KB reduced at various temperatures from the linear polarization curves in O_2-saturated 0.1 M $HClO_4$ electrolyte with a sweep rate of 5 mV/s and a rotation speed of 900 rpm.

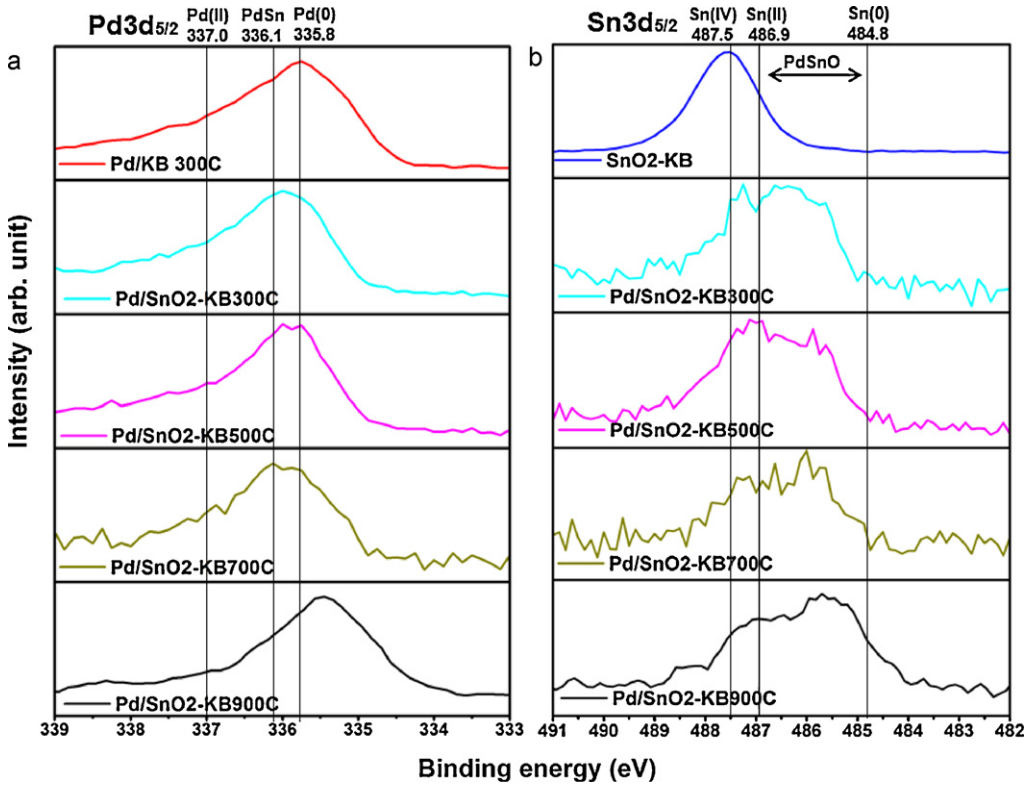

Fig. 4. XPS spectra of Pd/KB 300 °C, SnO_2/KB and Pd/SnO_2–KB reduced at various temperatures: (a) Pd 3d and (B) Sn 3d.

treated catalyst, the binding energy is shifted to higher values. However, there is a difference in the positive shift of binding energy of Pd/SnO_2–KB depending on the reduction temperature. The binding energy shifts of Pd/SnO_2–KB 300 °C and 500 °C originate from the partially oxidized surface Pd, because these catalysts include no intermetallic Pd_3Sn as in Fig. 1. Pd/SnO_2–KB 700 °C shows a more positive binding energy centered at 336.1 eV than the catalysts reduced at 300 °C or 500 °C with this level of binding energy shift being reported for Pd–Sn phase [16]. Although a part of Pd/SnO_2–KB 900 °C is the intermetallic Pd_3Sn, the binding energy is shifted negatively due to the excessive sintering of Pd and the evolution of other species as seen in Fig. 1.

The SnO_2–KB composite shows the binding energy centered at 487.5 eV for Sn 3d in Fig. 4(b) where the binding energies of Sn(IV), Sn(II), Sn(0) and quasimetallic Sn state (denoted as PdSnO) are indicated [17,18]. The Sn 3d binding energy of SnO_2–KB is exactly in accordance with that of 20 nm size SnO_2 particles [19]. The broad peaks developing during the thermal reduction of Pd/SnO_2–KB can be interpreted as the collective sum of each peak of four Sn bonding states (SnO_2, SnO, metallic Sn and quasimetallic Sn). The quasimetallic state of Sn was also reported by Rotermund et al. who suggested the quasimetallic state of Sn resulting from the bond between dissociated oxygen and Sn atom on the intermetallic Pd–Sn [20].

As the reduction temperature increases, the metallic Sn and quasimetallic Sn states become prominent but the major Sn state at Pd/SnO_2–KB is quasimetallic up to 900 °C. Taking the Pd 3d and Sn 3d XPS spectra into account together, we conclude that Pd/SnO_2–KB 700 °C includes a larger amount of intermetallic Pd_3Sn than Pd/SnO_2–KB 900 °C and the highest oxygen reduction activity of Pd/SnO_2–KB 700 °C is partly due to the intermetallic Pd_3Sn as a major surface species.

The surface composition of Pd/SnO_2–KB was investigated by XPS quantitative analysis. The atomic ratios of oxygen to metal (Pd + Sn) and of Pd to Sn are calculated as displayed in Fig. 5. Pd/SnO_2–KB 700 °C shows the highest O/(Pd + Sn) ratio and the lowest Pd/Sn ratio, which means that quasimetallic PdSnO is dominating on the Pd_3Sn intermetallic surface compared to Pd/SnO_2–KB reduced at other temperatures. The values of O/(Pd + Sn) ratio quantitatively include an uncertainty because of an additional source of surface oxygen atoms other than at PdSnO such as surface oxygen atoms on carbon, which has very large surface area compared to the metal particles and is a major component of the catalyst. Although the values of O/(Pd + Sn) ratio could be overestimated due to the oxygen atoms on carbon, they can be qualitatively matched with the XRD analysis in Fig. 1 such that the abrupt decrease in the ratio of Pd/SnO_2–KB 900 °C is expected with the emerging phase of Pd_2O of which O/Pd ratio is 0.5.

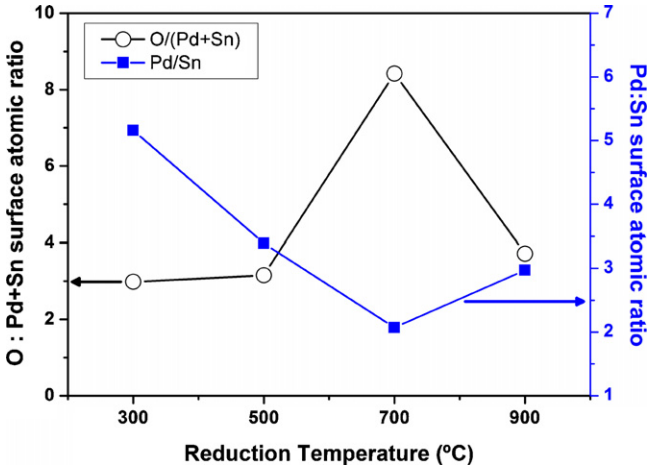

Fig. 5. Surface atomic ratios of oxygen to metal (Pd + Sn) and of Pd to Sn at Pd/SnO_2–KB reduced at various temperatures.

Miah et al. reported that Pd–Sn alloy showed an increased oxygen reduction activity due to Sn donating electrons to Pd, which increased the O_2 adsorption affinity of Sn [3]. The electron donation from neighboring Sn atoms to Pd atoms in the intermetallic Pd_3Sn can decrease the oxygen binding energy on Pd and the reduction of oxygen binding energy on noble metals including Pd can improve the activity for the oxygen reduction [1]. The enhanced oxygen dissociation and reduction activity are attributed to the combined effect of the decreased oxygen binding energy of Pd and increased O_2 adsorption affinity.

4. Conclusions

The intermetallic compound of Pd and Sn was synthesized by using the sequential impregnation method and successive reduction treatment at different temperatures and its oxygen reduction electrocatalytic activity was investigated. All samples were characterized by TEM, XRD, XPS and electrochemical half cell analysis. The Pd catalysts supported on tin oxide–carbon composite (Pd/SnO_2–KB) reduced at 700 °C and 900 °C clearly exhibited the Pd–Sn intermetallic compound with an expanded unit cell structure of Pd. The oxygen reduction electrocatalytic activity was correlated with the surface composition of the intermetallic compound. The catalyst treated at 700 °C among Pd/SnO_2–KB series showed the highest activity, which was attributed to the largest amount of quasimetallic PdSnO on the intermetallic compound surface.

References

[1] J.K. Norskov, J. Rossmeisl, A. Logadottir, J.R. Kitchin, T. Bligaard, H. Jonsson, J. Phys. Chem. B 108 (2004) 17886–17892.
[2] M. Friedrich, M. Armbrster, Chem. Mater. 21 (2009) 5886–5891.
[3] M.R. Miah, M.T. Alam, T. Okajima, T. Ohsaka, J. Electrochem. Soc. 156 (2009) B1142–B1149.
[4] A. Sarkar, A.V. Murugan, A. Manthiram, J. Mater. Chem. 19 (2009) 159–165.
[5] O. Savadogo, K. Lee, K. Oishi, S. Mitsushima, N. Kamiya, K.I. Ota, Electrochem. Commun. 6 (2004) 105–109.
[6] W. Tang, G. Henkelman, J. Chem. Phys. 130 (2009) 194504.
[7] Y. Xiong, H. Cai, B.J. Wiley, J. Wang, M.J. Kim, Y. Xia, J. Am. Chem. Soc. 129 (2007) 3665–3675.
[8] J.W. Guo, T.S. Zhao, J. Prabhuram, R. Chen, C.W. Wong, J. Power Sources 156 (2006) 345–354.
[9] P.K. Shen, C.W. Xu, R. Zeng, Y.L. Liu, Electrochem. Solid-State Lett. 9 (2006) A39–A42.
[10] Z. Zhang, X. Wang, Z. Cui, C. Liu, T. Lu, W. Xing, J. Power Sources 185 (2008) 941–945.
[11] S. Beak, D. Jung, K.S. Nahm, P. Kim, Catal. Lett. 134 (2010) 288–294.
[12] E. Casado-Rivera, D.J. Volpe, L. Alden, C. Lind, C. Downie, T. Vazquez-Alvarez, A.C.D. Angelo, F.J. DiSalvo, H.D. Abruña, J. Am. Chem. Soc. 126 (2004) 4043–4049.
[13] J. Greeley, I.E.L. Stephens, A.S. Bondarenko, T.P. Johansson, H.A. Hansen, T.F. Jaramillo, J. Rossmeisl, I. Chorkendorff, J.K. Norskov, Nat. Chem. 1 (2009) 552–556.
[14] T. Takeguchi, W. Ueda, 19th CRC International Symposium E8, 2007.
[15] W.J. Zhou, J.Y. Lee, J. Phys. Chem. C 112 (2008) 3789–3793.
[16] S. Nemšák, K. Mašek, V. Matolín, Surf. Sci. 601 (2007) 4475–4478.
[17] N. Kamiuchi, H. Muroyama, T. Matsui, R. Kikuchi, K. Eguchi, Appl. Catal. A: Gen. 379 (2010) 148–154.
[18] D. Briggs, M.P. Seah, Practical Surface Analysis, 2nd ed., Wiley, New York, 1990.
[19] Y. Wang, C. Ma, X. Sun, H. Li, Nanotechnology 13 (2002) 565–569.
[20] H.H. Rotermund, V. Penka, L.A. DeLouise, C.R. Brundle, J. Vac. Sci. Technol. A5 (1987) 1198–1202.